Study of the localization of electron in array of quantum rings

by

Rhiddha Acharjee

Roll: **21642410**

Registration No. **1061911400093 of 2019**

M. Sc. Semester-IV student
Department of Physics (Post-graduate)
Acharya Prafulla Chandra College, New Barrackpore

Under the guidance of

Dr. Atanu Nandy
Department of Physics
Acharya Prafulla Chandra College, New Barrackpore

Submitted for the partial fulfilment of the degree of
Master of Science in Physics

Acharya Prafulla Chandra College
New Barrackpore, Kolkata 700 131

"The more we study the major problems of our time, the more we come to realize that they cannot be solved without a deep understanding of solid-state physics."

— Richard Feynman

ACKNOWLEDGEMENTS

I want to acknowledge and express my immense gratitude to **Dr. Atanu Nandy**, Assistant Professor of Physics, Acharya Prafulla Chandra College, New Barrackpore, for giving me the opportunity to work on this project and guiding me throughout this work. I am also grateful for the facilities provided by this reputed physics department. I am also grateful and feeling blessed to my **parents and my sister** for their love and support.

Signature of candidate

Dedicated to my parents, my sister and Dr. Atanu Nandy

Phone: 2537-3297 / 8797
E-mail:*apc1960@apccollege.ac.in*
www.apccollege.ac.in

Acharya Prafulla Chandra College
(NAAC ACCREDITED 'A' GRADE COLLEGE) (Govt. Sponsored)
P.O. New Barackpore, North 24 Parganas, Kolkata-700 131, West Bengal

To Whom It May Concern

This is to certify that **Rhiddha Acharjee (Roll No: 21642410 and Registration No. : 1061911400093 of 2019)**, a postgraduate student in the Department of Physics of Acharya Prafulla Chandra College, has carried out his M. Sc. project entitled **"Study of the localization of electron in array of quantum rings"** under my supervision in connection with the M. Sc. Physics 4^{th} semester examination-2024. He has completed the project, and the report is now ready for submission.

I wish him good luck in his future endeavors.

Date: 23.08.2024

Signature of the Supervisor

ABSTRACT

Our main discussion is about to study the spectral properties of low dimensional systems using some externally controllable physical quantity. The localization aspect of an array of quantum rings is studied in details within the tight-binding framework. It is very interesting to point out that the spectral landscape of the system can be tuned by some external magnetic flux. We have taken array quantum rings coupled axially or in transverse direction for the study of localization. The density of single particle eigenstates is determined by the numerical evaluation of density of states is determined by the numerical evaluation of density of states, inverse participation ratio and the band dispersion by virtue of real space decimation technique and Green's function approach.

Contents

Introduction

Low dimensional quantum systems have been of intense research in theory and experiments, due to the fact that these simple-looking systems are prospective candidates for nano devices in electronic and spintronic engineering. Apart from this feature, several striking spectral properties are exhibited by such systems owing to the quantum interference which is specially observed in quantum networks containing closed loops.
Examples are the Aharonov-Bohm AB in the magneto conductance of quantum dots, electron transport in quantum-dot arrays, Fano effect in a quantum ring quantum dot system, spin-filter effects in mesoscopic rings, and dots to name a few. Recently, Aharony proposed a model of a nano-spintronic device using a linear chain of diamond-like blocks of atomic sites [1]. Each plaquette of the array is threaded by identical magnetic flux. They have analyzed how the Rashba spin-orbit interaction and the AB flux combine to select a propagating ballistic mode. A similar chain was earlier investigated by Bercioux [2] in the context of spin-polarized transport of electrons and by Vidal and Doucot [3] and Vidal to study two interacting particles, and Josephson junction chain of diamonds, both in the presence of a magnetic field. However, there are certain special spectral features offered by the diamond chain, particularly, the role of the AB flux, which we believe,remain unexplored. This is precisely the area we wish to highlight in the present communication. We show that an infinite diamond chain of identical atoms behaves as an insulator at $T = 0$ K in the presence of a nonzero AB flux. As we arrange atoms of two different kinds represented by two different values of the on-site potential periodically on a diamond chain, a highly degenerate localized level is created near one of the two subbands of extended states. The proximity of this localized level to either of the subbands can be controlled by tuning the AB flux and can be made to stay arbitrarily close to either of the subbands. The entire system is then capable of behaving as an n-type or a p-type semiconductor as explained later. The conductance spectrum of a finite array of the diamond plaquettes is also studied to judge the applicability of such a network geometry in device engineering.

A. Localization of excitation

The study of the nature of the single-particle eigenstates in low-dimensional quantum networks has always been an interesting topic in condensed matter physics. If an electron moves under the influence of a periodic potential then wave function is a perfectly extended one,and is generally termed as the Bloch wave function [4]. For a one-dimensional repetitive arrangement of potentials which can be typically represented as:

$$V(x) = V(x \pm a) \tag{1}$$

where a is the lattice periodicity, the Bloch wave functions have the form:

$$\psi_k(x) = u_k(x)e^{\pm ikx} \tag{2}$$

Here, $u_k(x)$ is the modulating factor which has the same periodicity as that of the lattice. The complete reverse scenario is seen when an electron moves in a disordered environment,

say in an arrangement of random scatterers(e.g., impurities). Owing to the multiple number of scatterings, its diffusive motion gets stopped in space. We thus observe a complete absence of diffusion of wave packet particularly in one dimension irrespective of the strength of the disorder. This path-breaking phenomenon was first brought to notice by P.W. Anderson, and is known as *Anderson localization* [5].

The single-particle eigenstates get exponentially localized in an array of scatterers for any arbitrary amount of random and uncorrelated disorder in the distribution of on-site potentials. After this pioneering work by Anderson, it was also shown via scaling theories of localization [6] that all single-electron states are exponentially localized even in two dimensions, independent of the strength of disorder in case of non-interacting electrons, although a possibility of metal-insulator transition was proposed in case of three dimensions.

B. Flat band localization

Since the particles 'residing' on a flat band do not possess kinetic energy, they do not contribute to transport. The physical reason behind the overall transmission corresponding to flat band mode across a full lattice being practically zero is the local geometric phase cancellation at the connector nodes. This means that the "energy" is trapped as a direct consequence of consecutive destructive kinds of quantum interference occurred by the multiple quantum dots. The non-zero amplitudes may be confined within the characteristic trapping cell and one such finite cluster is isolated from the other cluster by a special set of sites on which the amplitude of the wave function is zero. This immediately implies the immobility of the wave train as it eventually gets trapped inside the finite cluster of that sites. Thus the extremely low or even zero group velocity of the particle corresponding to such self-localized states eventually contributes to the non-dispersive signature. Due to macroscopic degeneracy, any superposition of those states is completely static, displaying no evolution dynamics. Recent authentic experimental observation of localized flat band modes in a quasi-one dimensional photonic rhombic lattice in the tight-binding framework makes the study of flat band model networks more challenging. In case of periodic systems the spectrum always carries a dispersive signature due to the presence of Bloch-like eigen-states and hence the energy will diffuse only (except certain k points where the group velocity becomes locally zero). By virtue of this, for single mode excitation,a set of linear delocalized modes with different spatial frequencies will be excited and waves will propagate without spatial coherence across the network. Therefore, we do not observe the stationary localized modes for periodic linearly standard geometry. But for flat band systems one can easily observe strong localization which is dependent on the lattice topology itself and it does not need any external parameter. The additive destructive interference will make possible the cancellation of the amplitude at the connecting nodes and the transport will be just forbidden. Diffusion of quantum mechanical wave packets is suppressed due to the presence of disorder in the system. This is the pioneering result of Anderson. But several low dimensional geometries are there, in where single particle eigenstates can be localized even when there is no disorder in the site potential or in the overlap integral. The destructive wave interference by virtue of the lattice topology makes this possible to happen in many quasi-one-dimensional geometries like kagomé, lieb, diamond, stub, saw-tooth lattices etc. This is the essence of flat band localization.

C. Experimental support

This phenomenon, originally observed in electronic systems [7], has since expanded its relevance across various fields within condensed matter physics, extending far beyond it's initial electronic context. The concept of excitation localization has evolved and is no longer limited to electronic scenarios alone. In recent decades, significant attention has been focused on experimental studies of localization. These studies span from the localization of classical waves [8], such as light [9, 10, 11, 12], acoustic waves [13, 14, 15], and microwaves [16, 17] in random media, to the latest developments in photonic localization. Such advances have allowed for experimental testing of Anderson localization using custom-designed lattices. Crucially, the challenges related to inelastic scattering and other effects like electron-electron and electron-phonon interactions do not significantly hinder the experimental observation of wave localization.
The advent of nanotechnology and lithography has further facilitated the direct observation of classical wave localization. Recently, several research groups have reported experimental evidence of light localization in disordered media [18], ultrasound localization in three-dimensional elastic networks [19, 20], and matter wave localization using a Bose-Einstein condensate in a one-dimensional disordered optical potential [21]. These experimental results align well with the theoretical framework of wave localization that has been developed over the years.

D. The Aharonov-Bohm effect

The Aharonov-Bohm effect [22] is a quantum mechanical phenomenon in which an electrically charged particle is affected by an electromagnetic potential (Φ, $\mathbf{A}$), despite being confined to a region in which both the magnetic field $\mathbf{B}$ and electric field $\mathbf{E}$ are zero. The underlying mechanism is the coupling of the electromagnetic potential with the complex phase of a charged particle's wave function, and the Aharonov-Bohm effect is accordingly illustrated by interference experiments [23]. The most commonly described case, sometimes called the Aharonov-Bohm solenoid effect, takes place when the wave function of a charged particle passing around a long solenoid experiences a phase shift as a result of the enclosed magnetic field, despite the magnetic field being negligible in the region through which the particle passes and the particle's wave-function being negligible inside the solenoid. This phase shift has been observed experimentally. There are also magnetic Aharonov-Bohm effects on bound energies and scattering cross sections. An electric Aharonov-Bohm phenomenon was also predicted, in which a charged particle is affected by regions with different electrical potentials but zero electric field, but this has no experimental confirmation yet. We consider the Aharonov-Bohm phase which turns out to be also a special case of general Berry phases. Mathematically, we describe this by including a potential $U(x)$ in the Hamiltonian that is infinite outside the box. By calling the box 'small' we mean that the gauge potential is approximately constant inside the box. In order for the magnetic field to approximately vanish outside the solenoid, we take the solenoid to be very large in the direction perpendicular to the image plane. At position $\mathbf{x} = \mathbf{X}$,then the Hamiltonian reads,

$$H = \frac{1}{2m}[\vec{p} - \frac{e}{c}\vec{A}(\vec{X})]^2 + U(\vec{x} - \vec{X}) = \frac{1}{2m}[-i\hbar\nabla - \frac{e}{c}\vec{A}(\vec{X})]^2 + U(\vec{x} - \vec{X}) \qquad (3)$$

We now place the center of the box at a position $\mathbf{x} = \mathbf{X}_0$ where the gauge potential vanishes. This can always be done due to gauge freedom. The solution to the Hamiltonian is now just the solution of a particle in a box and we denote the ground state solution by $\psi_(\vec{x} - \vec{X_0})$.

In specifying this wave function, we have also made a choice of the phase. The connection to Berry phases becomes evident when doing the following: We slowly move the box in some path in space. On this path, the gauge potential experienced by the particle changes. The Schrödinger equation for the Hamiltonian is then solved by the state-

$$\psi(\vec{x} - \vec{X}) = \exp\left(\frac{ie}{\hbar c}\int_{\vec{X_0}}^{\vec{X}} \mathbf{A}(\vec{x'}) \cdot d\vec{x'}\right)\psi(\vec{x} - \vec{X_0}) \tag{4}$$

This is because when the gradient ∇ acts on the exponent, it pulls down a factor which cancels the $\frac{e\vec{A}}{c}$ term. To obtain the Berry phase, we take the box in a loop C and bring it back to where we started. Our original wave function thereby catches a phase:

$$\psi(\vec{x} - \vec{X_0}) = \exp(i\gamma)\,\psi(\vec{x} - \vec{X_0}) \tag{5}$$

with,

$$\gamma = \frac{e}{\hbar c}\oint_C \mathbf{A}(\tilde{\mathbf{x}}) \cdot d\vec{x} \tag{6}$$

Comparing this to our general expression for the Berry phase, we see that in this particular context, the Berry connection is actually identified with the electromagnetic vector potential,

$$\mathbf{A}(\vec{X}) = -\frac{e}{\hbar c}\vec{A(\vec{x}} = \vec{X}) \tag{7}$$

A particle of arbitrary charge q that goes around a region containing flux Φ will pick up an Aharonov-Bohm phase

$$\exp\left(\frac{iq\Phi}{\hbar}\right) \tag{8}$$

Recent experiments conducted by Yamamoto et al. [24] have sparked further exploration into quantum transport within AB interferometers. Additionally, earlier theoretical models have significantly contributed to understanding the key characteristics of electronic states and coherent transport in quantum network models, particularly within low-dimensional systems [25, 26, 27]. Advances in growth, fabrication, and lithography techniques have enabled the creation of custom-designed lattice structures using quantum dots (QD) or Bose-Einstein condensates (BEC), which hold great promise for applications in device technology. Consequently, these developments have also driven substantial theoretical research into model quantum networks with complex topologies [28, 29].

Methodology

A. Tight Binding Hamiltonian

We start our description from the [**fig-1(a)**] where a portion of an infinitely extended axially coupled quantum rings is shown pictorially. The system is governed by the standard tight-binding Hamiltonian, written in the Wannier basis, for non-interacting electrons, viz.,

$$H = \sum_i \epsilon_i |i\rangle\langle i| + \sum_{\langle ij \rangle} t_{ij} |i\rangle\langle j| \;\; e^{i\Phi_{ij}} + \text{h.c.} \tag{9}$$

Where ϵ_i denotes the onsite potential of i^{th} lattice point,t_{ij} represents the overlap integral that signifies the kinetic information for i^{th} and j^{th} nodes. It is to be noted that we consider only the interactions among the nearest neighboring atomic sites. The onsite potential of each lattice point is considered to be ϵ= 0 and the hopping integral taken as unifromity (t=1) throughout the numerical workout. The choice of the numerical values of the parameters of the Hamiltonian is of course arbitary and the overall spectral feature should not depend on that choice. Hence we have maintained uniformly in this choice and we assume that no serious physics-wise information is lost with such selection.

B. The Decimation Scheme

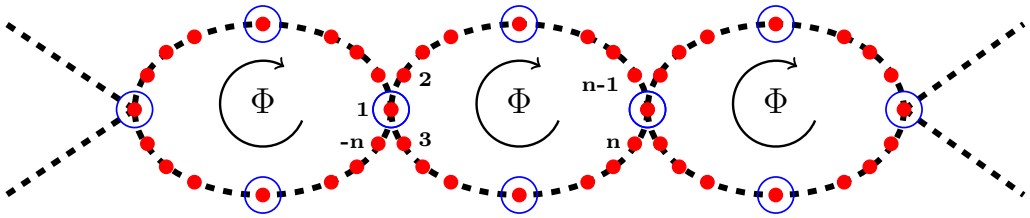

Figure:1(a) Schematic diagram of axially coupled diamond ring with N number of atomic sites in each arm of the diamond

Now we can write the discretized form of the Schrödinger equation(also termed as difference equation) for our prescribed lattice system:

$$(E - \epsilon_i)\psi_i = \sum_j t_{ij}\psi_j \tag{10}$$

It is seen from the [**fig-1(a)**] that each arm of the diamond shaped quantum ring contains N number of atomic sites such that the total number of sites in a particular ring is **4(N+1)**. A uniform magnetic flux Φ is enclosed by each ring. With the help of real space decimation formalism, we will eliminate the wave amplitudes of an appropriate of atomic sites in terms of other surviving nodes(marked by the dotted circle) such that the ring transform into an effective diamond-shaped structure as depicted in the [**fig-1(b)**]. The effective ring may be described by effective parameters. Now our network [**fig-1(a)**] transformed to [**fig-1(b)**]. The parameters are demonstrated as follows:
where,

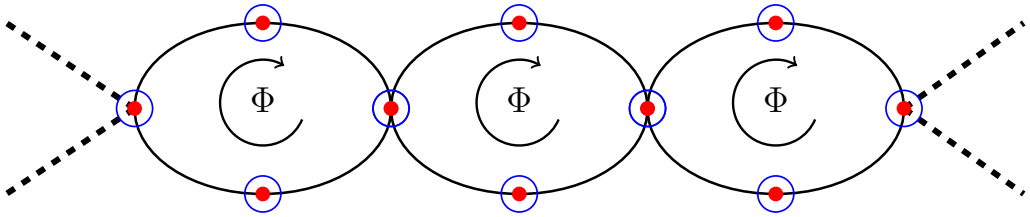

Figure-1(b) The renormalized array of axially coupled array of quantam chain with N number of atomic sites in each arm of the diamond ring

the effective onsite potential:

$$\tilde{\epsilon} = \epsilon + 2t\frac{U_{\text{N-1}}}{U_N} \tag{11}$$

the effective hopping integral:

$$\tilde{t_F} = \frac{te^{i(N+1)\theta}}{U_N} \tag{12}$$

$$\tilde{t_B} = \frac{te^{-i(N+1)\theta}}{U_N} \tag{13}$$

where,

$$\theta = \frac{2\pi\Phi}{4(N+1)\Phi_0} \tag{14}$$

here, $\tilde{t_f}$ is the effective forward hopping and $\tilde{t_b}$ is the effective backward hopping integral **(see Appendix: A for details)**, and U_N is the chebyshev polynomial(second kind) of N^{th} order **(see Appendix: B for details)**.

It is necessary to mention that the real space decimation methodology we have employed here is completely mathemathical construction. We are nothing doing with the original lattice. Moreover, the analytical formalism although is presented in a position of an infinite network but it is happening globally throughout the entire system. This mathematical mapping does not change the physics. To the best of our knowledge, this transformation scheme can be applied to any kind of quasi-one dimensional systems.

Results and analysis

We divide our results and analysis in two segments. First we try to focus on the spectral property offered by axially coupled quantum rings and their same rings coupled in transverse direction and extended axially. The general spectral landscape along with the calculation of density of states, inverse participation ratio and the band dispersion. We examine the general character of energy spectrum of **(a) axially coupled** and **(b) transversely coupled array of quantum rings**, when each elementary plaquette is threaded by an uniform magnetic flux Φ. The presence of magnetic field breaks the time reversal symmetry of the electron hopping along a band and it is taken care by introducing Peierl's phase in the hopping integral, viz., $\mathbf{t} \rightarrow \mathbf{t}\ exp[\frac{iq}{\hbar c}\int \vec{A}\cdot\vec{dr}]$. This is the basic essence of Aharnov-Bohm(AB) effect.

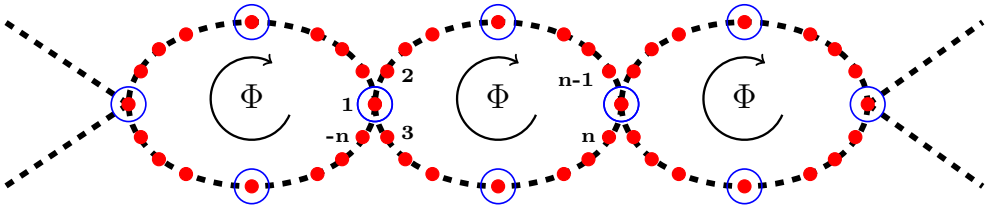

Figure: 2(a) Schematic diagram of an axially coupled array of quantam chain with number of atomic sites= N in each arm of diamond ring threaded by flux Φ in each plaquette

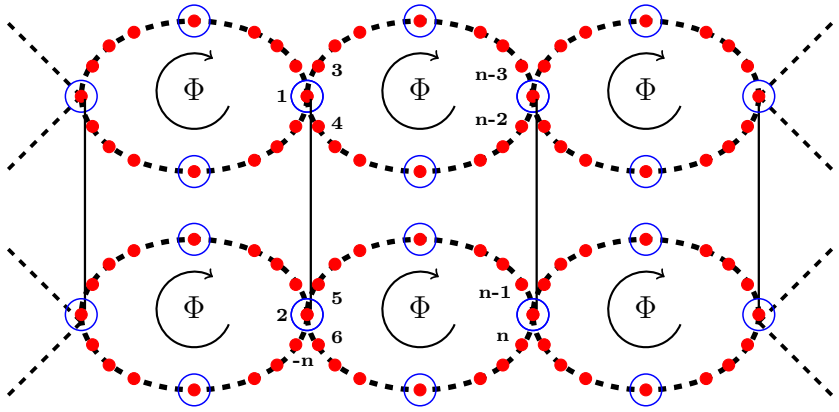

Figure:2(b) Schematic diagram of transverse coupled array of quantam chain with number of atomic sites= N in each arm of diamond ring threaded by flux Φ in each plaquette

When an electron goes round a closed loop that traps a magnetic flux Φ, it's wavefunction gains a phase. At this point, it is pertinent to remark that the Peierls' substitution **(see Appendix: C for details)**, though widely used to describe tight binding electrons under a magnetic field, is valid if the vector potential is slowly varying and there is no ambiguity of path along which the line integral is evaluated [30]. In the present work, we evaluate the line integral along the straight line connecting two nearest neighbouring sites and the vector potential is taken to be constant over a distance at least one lattice constant. Therefore, no serious problem is caused by the peierls' substitution in present case. This may be considered an analogous dispersion relation because for an electron moving around a closed path, it is well known that the magnetic flux plays the similar physical role as that of wave vector. Endless periodic array of (I) axially coupled **(Fig: 2.a)** and (II) transversly coupled binary fashioned diamond shaped network **(Fig: 2.b)**

(With N= odd and even interatomic site in each arm) which is suitable for studying the aspect of spinfilter is capable of behaving a semiconductor depending on a subtle choice of onsite potential and the strenght of magnetic flux threading each elementary plaquette.

A. Discussion of density of states

The expression for the local density of states as follows:

$$\rho_{00}(E) = \lim_{\eta \to 0^+} \left[-\frac{1}{\pi} \mathrm{Im}(G_{00}(E + i\eta)) \right] \tag{15}$$

where $\rho_{00}(E)$ is the density of state and the tight-binding Green function is $G_{00}(E + i\eta)$ **(see Appendix: D for details)**. Green's function can be written as,

$$G_{00}(E) = \frac{1}{N} \sum_k \frac{1}{E - \epsilon(k)} \tag{16}$$

$$\Rightarrow G_{00}(E + i\eta) = \frac{1}{N} \sum_k \frac{1}{E + i\eta - \epsilon(k)} \tag{17}$$

A small imaginary part is added to the energy in density of states calculations to simulate the broadening of energy levels and ensure numerical stability. Using the (15) the E-ρ relationship is plotted. The results are shown for odd ($N = 1$) and even ($N = 2$) numbers of sites in each arm of the diamond shaped quantum ring. It is needless to say that the entire analysis is possible for any large value of N. One general comment we can do is that with the increase of N, the spectrum will become more fragmented. As it is observed that in absence of magnetic perturbation, the density of states spectrum consists of a central absolutely continuous band with a central spike and two other subbands at the flanks. The central absolutely continuous band is populated by resonant kind of eigenfunctions. For any of the energy belonging to the continuum zone the hopping integral between the nearest neighbors does not decay which is a key signature of the state being extended. In other words, the if the incoming projectile carries any of such energies then the entire system behaves as transparent to the incoming electron leading to a high transmission probability. The central spike gives a message of compact localization but as it lies within the continuum, one cannot identify the localization character of the state.

As in the case of simple diamond network, in this case also a nominal magnetic flux introduces a gap at the central regime and it separates the central flat band from the continuous band. The magnetic flux thus helps us to mark the localization character of the state at $E = 0$. The second plot is for $\Phi = \frac{\Phi_0}{4}$. For the central flat band state as noticed in the density of states profile, the non-vanishing amplitudes are confined within a finite size cluster of atomic sites, known as *characteristic trapping cell* and one such cluster is effectively decoupled from the similar cluster by some node with zero amplitude. This is solely responsible for quenched kinetic information of the wave packet corresponding to the energy $E = 0$.

However, when we set $\Phi = \frac{\Phi_0}{2}$, the density of states spectrum consists of number distinct non-resonant localized modes. The reason is obvious. At such special flux value, the effective connectivity between the two axial extremities vanishes. This complete absence of diffusion is known as extreme localization of eigenstates. This is also a special subset

of Aharonov-Bohm caging that commonly happens in any flux induced quasi-one dimensional network. The corresponding eigenstate is localized in space either at some selected node or a very tiny cluster of atomic sites.

I. Axially coupled array of quantam rings

Case-A

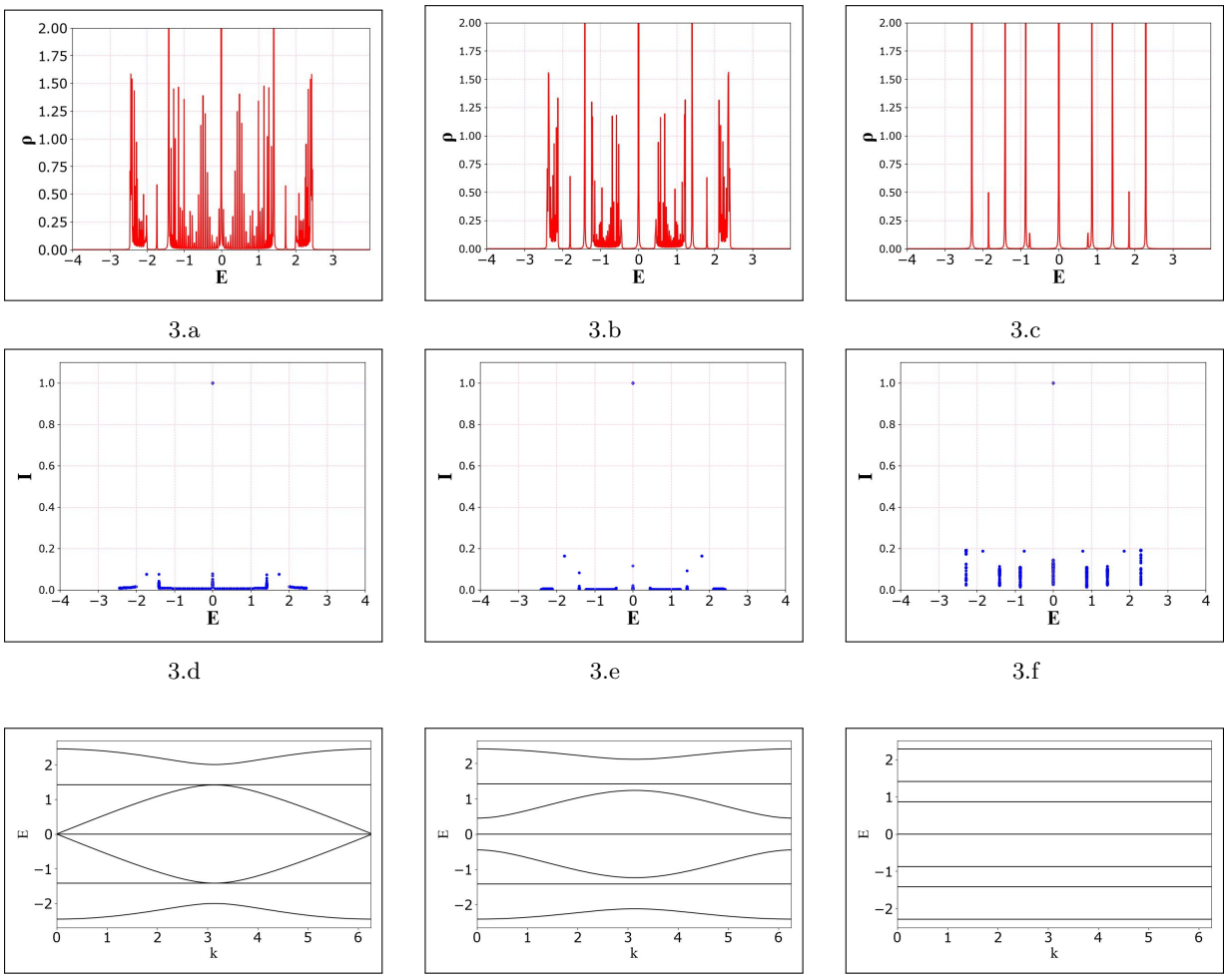

3.a 3.b 3.c

3.d 3.e 3.f

3.g 3.h 3.i

Figure:3 (Upper panel) Variation of density of states with respect to the energy of electron for the axially coupled array of diamond chain with uniform magnetic flux Φ (in units of $\Phi_0 = \frac{hc}{e}$, threaded by each plaquette, the value of the magnetic flux is (a) $\Phi = 0$ and (b) $\Phi = \frac{1}{2}\Phi_0$ and (c)$\Phi=\frac{1}{4}\Phi_0$, total number of atomic sites is 701 for plotting **(middle panel)** variation of inverse participation ratio with energy, flux values are same as mentioned in the upper panel, total number of atomic sites is 701 for plotting **(lower panel)** dispersion relation(i.e.relation between energy and wave vector), flux values are same as mentioned in the upper panel; number of atomic sites along each arm of the diamond is N=1; range of k is 0 to $+2\pi$ and 500 values of k is generated within this range

Case- B

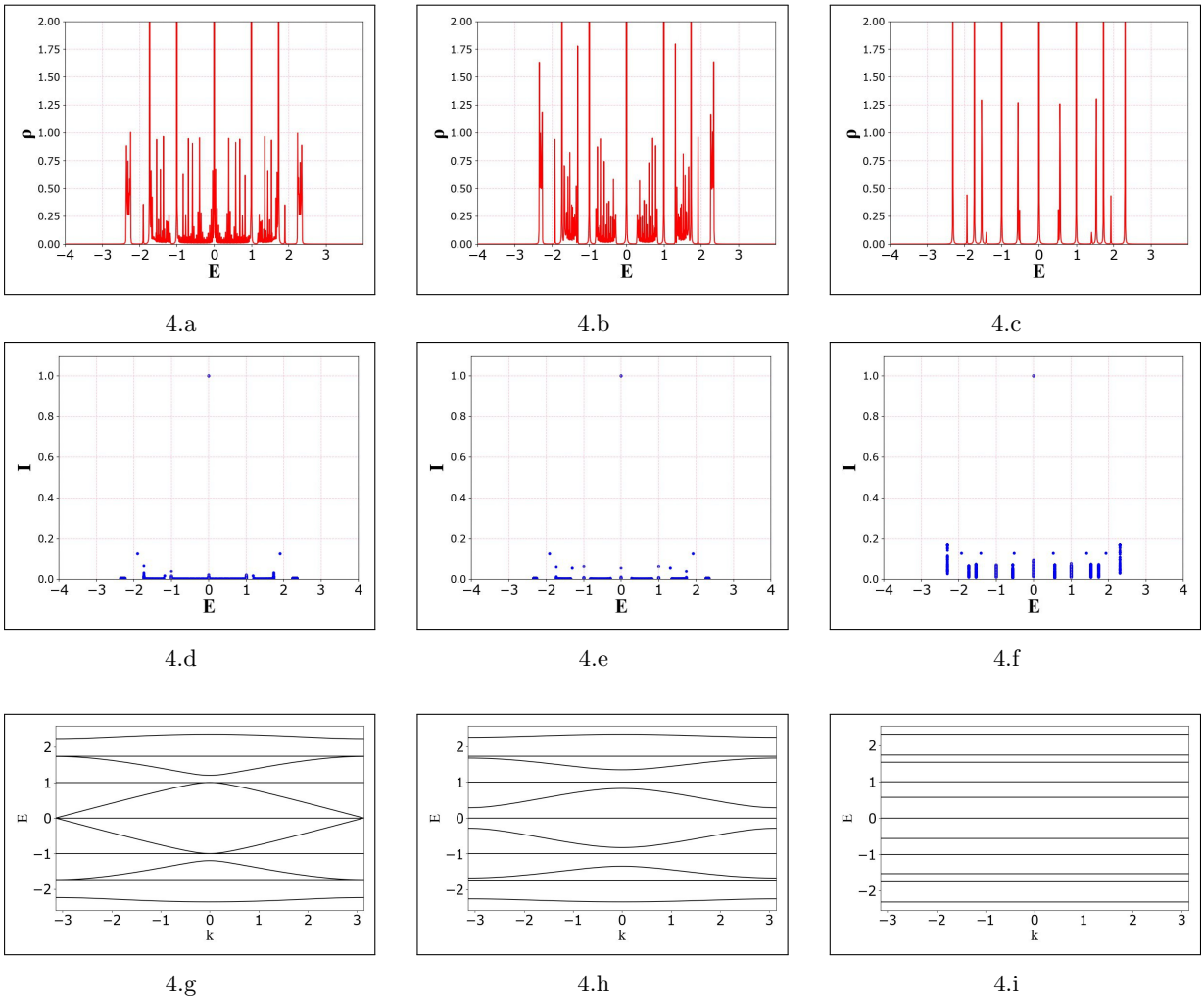

4.a 4.b 4.c

4.d 4.e 4.f

4.g 4.h 4.i

Figure:4 (Upper panel) variation of density of states with respect to the energy of electron for the axially coupled array of diamond chain with uniform magnetic flux Φ (in units of $\Phi_0 = \frac{hc}{e}$, threaded by each plaquette, value of the magnetic flux is (a) $\Phi = 0$ and (b) $\Phi = \frac{1}{2}\Phi_0$ and (c)Φ=$\frac{1}{4}\Phi_0$; total number of atomic sites is 1101 for plotting **(middle panel)** variation of inverse participation ratio with energy, the flux values are same as mentioned in the upper panel; total number of atomic sites is 1101 for plotting **(lower panel)** dispersion relation(i.e. relation between energy and wave vector), flux values are same as mentioned in the upper panel; number of atomic sites along each arm of the diamond is N=2; range of k is -π to +π and 500 values of k is generated within this range

B. Discussion of Inverse participation ratio

For sake of completeness of the above discussion, we have also computed the inverse participation ratio (IPR) as a function of energy E of the incoming excitation.

$$\mathrm{IPR}(E) = \frac{\sum_n |\psi_n(E)|^4}{\left(\sum_n |\psi_n(E)|^2\right)^2} \tag{18}$$

Maximum possible value of inverse participation ratio approaches to one for localised state for an extended state, vanishing the very small in the large system size network. The relation between the typical density of state and the local density of states can be

given by similar to the localisation in disordered system. These order parameter is finite in the localised face and zero in the localised phase and goes to 0. At the transition. We have also calculated the inverse participation ratio for our periodic system to observe the effect of magnetic flux. The study of inverse participation ratio makes the study of spectral crossover more convincing from the experimental perspective.
The demonstration of inverse participation ratio plots is a supportive signature of localization information for this ring geometry. A complete set of plots which are consistent with the density of states profiles are observed in the middle panel. In presence of finite magnetic perturbation, the central resonant band bifurcates into two symmetric parts around the central energy $E = 0$. AB caging effect [31] is also observed in the inverse participation ratio pattern for half flux quantum.
For the even number of atomic sites in each arm, the same density of states and inverse participation ratio plots are cited. As we see that the central resonant window in absence of flux becomes wider than the previous case. The other fragmentation in presence of flux and extreme localization are also seen for this even number of quantum dots case also. Here we should appreciate ourselves that the flux tunability of the density of states spectrum is very much interesting in the context of fabricating some switching and other devices in the present era of advanced nanotechnology and lithographic techniques. The magnetic flux is an external parameter which can have a comprehensive control over the spectral landscape.

C. Discussion of dispersion relation

To workout the band dispersion relation,we need to transform the real space tight-binding Hamiltonian into momentum space. The basis states are related to the wannier states simply by a Fourier transform.
In momentum, space the Hamiltonian of the system can be cast by following relation:

$$H = \sum_k \psi_k^\dagger \mathcal{H}(k) \psi_k \tag{19}$$

We can use the above expression to obtain the Hamiltonian for any particular. For Axially coupled ring with the number of atomic sites in each arm of the diamond is N=1, the matrix is given by,

$$\mathcal{H}(k) = \begin{pmatrix} \epsilon & t_b & t_f & 0 & 0 & t_f e^{-ika} & t_b e^{-ika} \\ t_f & \epsilon & 0 & t_b & 0 & 0 & 0 \\ t_b & 0 & \epsilon & 0 & t_f & 0 & 0 \\ 0 & t_f & 0 & \epsilon & 0 & t_b & 0 \\ 0 & 0 & t_b & 0 & \epsilon & 0 & t_f \\ t_b e^{ika} & 0 & 0 & t_f & 0 & \epsilon & 0 \\ t_f e^{ika} & 0 & 0 & 0 & t_b & 0 & \epsilon \end{pmatrix} \tag{20}$$

K is the wave vector and a is the lattice constant. The dimension of Hamiltonian matrix depends on number of atom present in a unit cell of infinite network ϵ is the onsite potential which is ϵ**=0** in our study. For, (a) axially coupled array of quantum chain with the number of atomic sites along each arm of diamond → N=1 is (7 × 7) and for N=2 is (11 × 11) (b) transverse coupled array of quantum chain with the number of atomic sites along each arm of diamond → N=1 is (14 × 14) and for N=2 is (22 × 22). One can solve the charesterestic equation of Hamiltonian matrix, we get the energy eigen

value and dispersion relations are plotted. The spectrum turns out to be gapless for Φ= 0. As the flux gradually increases the gaps opens and at Φ= $\frac{1}{2}$, we get flat band states.

II. Transverse coupled array of quantam rings

Case- C

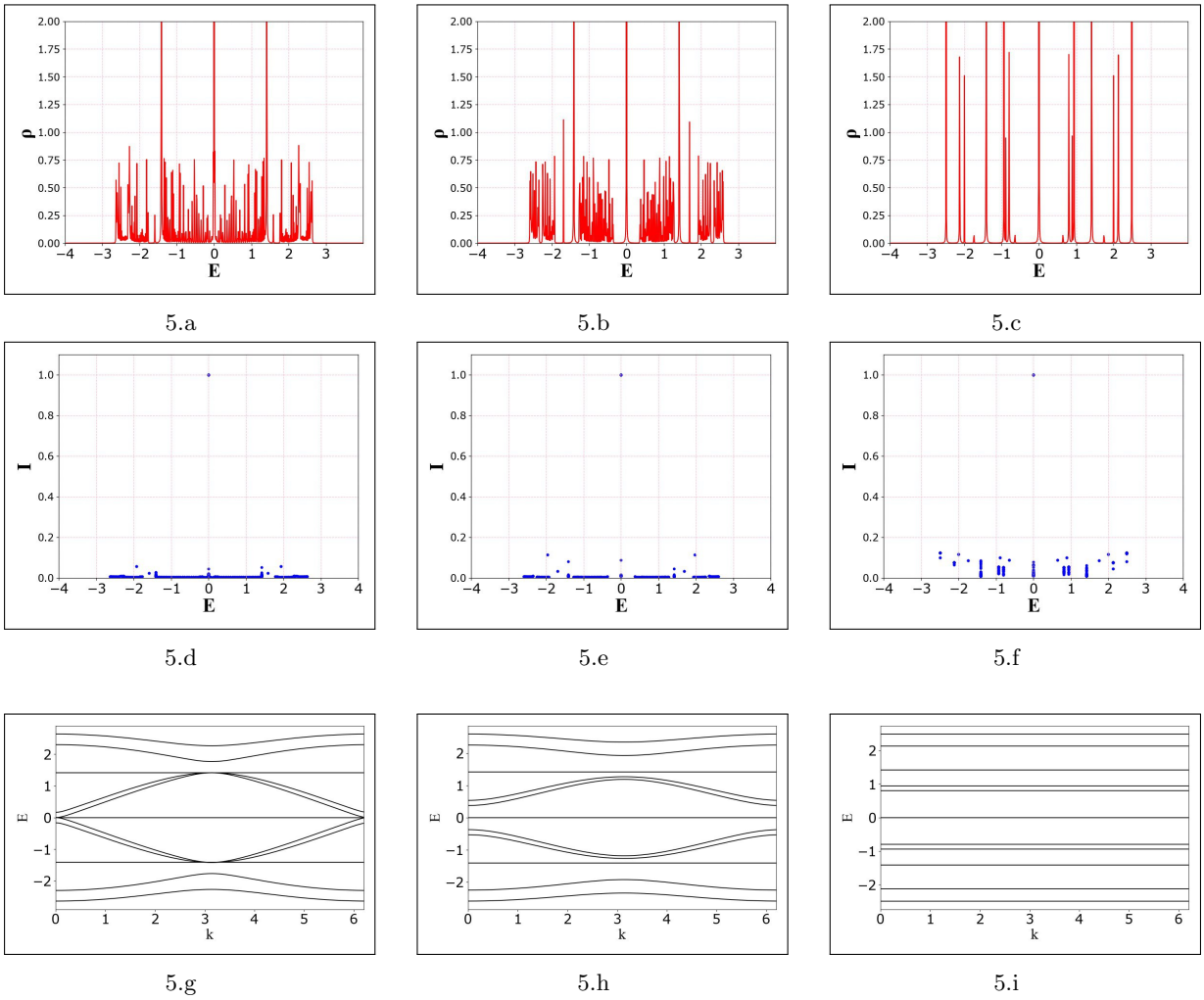

5.a 5.b 5.c

5.d 5.e 5.f

5.g 5.h 5.i

Figure:5 (Upper panel) variation of density of states with respect to the energy of electron for the transverse coupled array of diamond chain with uniform magnetic flux Φ (in units of $\Phi_0 = \frac{hc}{e}$, threaded by each plaquette, value of the magnetic flux is (a) Φ = 0 and (b) Φ = $\frac{1}{2}\Phi_0$ and (c)Φ=$\frac{1}{4}\Phi_0$, the total number of atomic sites is 982 for plotting **(middle panel)** variation of inverse participation ratio with energy, the flux values are same as mentioned in the upper panel, the total number of atomic sites is 982 for plotting **(lower panel)** dispersion relation(i.e.relation between energy and wave vector), the flux values are same as mentioned in the upper panel, the number of atomic sites along each arm of the diamond is N=1; the range of k is 0 to $+2\pi$ and 500 values of k is generated within this range

Case- D

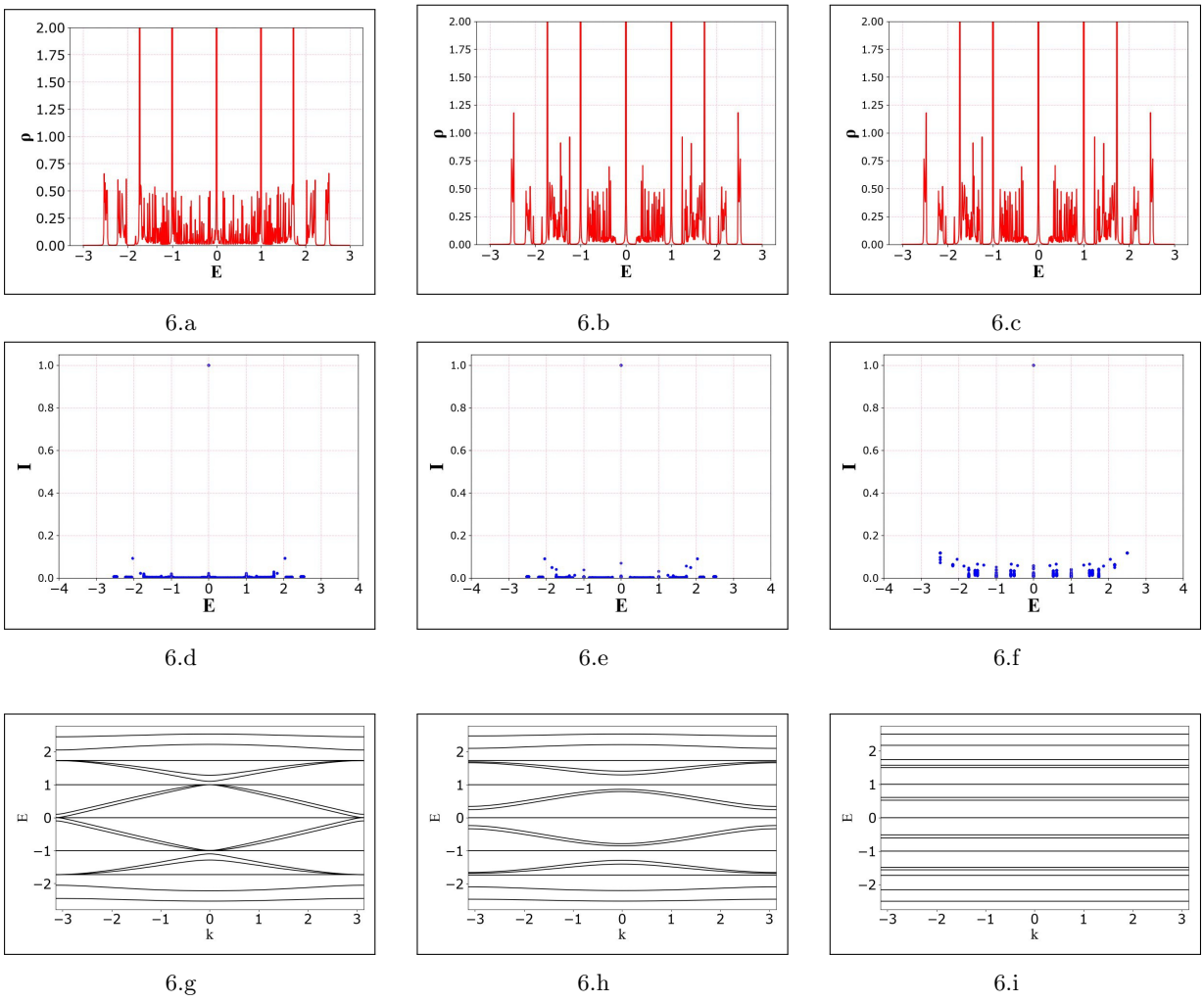

Figure:6 (Upper panel) variation of density of states with respect to the energy of electron for the transverse coupled array of diamond chain with uniform magnetic flux Φ (in units of $\Phi_0 = \frac{hc}{e}$, threaded by each plaquette, the value of the magnetic flux is (a) $\Phi = 0$ and (b) $\Phi = \frac{1}{2}\Phi_0$ and (c)Φ=$\frac{1}{4}\Phi_0$, the total number of atomic sites is 882 for plotting **(middle panel)** variation of inverse participation ratio with energy, the flux values are same as mentioned in the upper panel, the total number of atomic sites is 882 for plotting **(lower panel)** dispersion relation(i.e.relation between energy and wave vector), the flux values are same as mentioned in the upper panel, the number of atomic sites in each arm of the dimond chain is N=2; the range of k is -π to +π and 500 values of k is generated within this range

D. Eigenspectrum as a Function of Flux

As, for an electron circulating around a closed loop, the magnetic flux plays a role equivalent to the wave vector [32]. We examine the general character of the energy spectrum of quasi-one-dimensional diamond network when each elementary plaquette is threaded by a uniform magnetic flux Φ. The presence of a magnetic field breaks the time reversal symmetry of the electron hopping along a bond and this is taken care of by introducing a Peierls' phase in the hopping integral, viz., $t \rightarrow t \exp\left[(\frac{iq}{hc})\int \vec{A}\cdot d\vec{r}\right]$. This is the basic essence of Aharonov-Bohm effect. When an electron goes round a closed loop that traps

a magnetic flux Φ, it's wave function gains a phase. This simple sentence is at the heart of the path-breaking Aharonov-Bohm (AB) effect that has led to an extensive research in the so-called AB interferometry which dominated the physics, both experiments and theory, in mesoscopic dimensions over the past couple of decades. At this point, it is pertinent to remark that the Peierls' substitution, though widely used to describe tight binding electrons under a magnetic field, is valid if the vector potential is slowly varying and there is no ambiguity of the vector potential is slowly varying and there is no ambiguity of the vector potential if the magnetic field, is valid if the vector potential is slowly varying and there is no ambiguity of path along which the line integral is evaluated. In the present work, we evaluate the line integral along the straight line connecting two nearest neighboring sites and the vector potential is taken to be constant over a distance of at least one lattice constant. Therefore, no serious problem is caused by the Peierls' substitution in the present case. This diagram may be considered an analogous dispersion relation because for an electron moving round a closed path, it is well known that the magnetic flux plays the similar physical role as that of the wave vector. The central motivation behind this spectral study is that one can continuously engineer the magnetic flux to control the localization of wave train with high selectivity. Moreover, there are a number of inter-twined band overlap, and a quite densely packed distribution of allowed modes, forming quasi-continuous energy-flux band structure. The spectrum is of course flux periodic, as expected. The overall allowed eigenspectrum with respect to the external magnetic perturbation is plotted for different cases. The pattern is of course flux periodic due to the flux dependence of effective overlap integral through the ChebyShev polynomial.

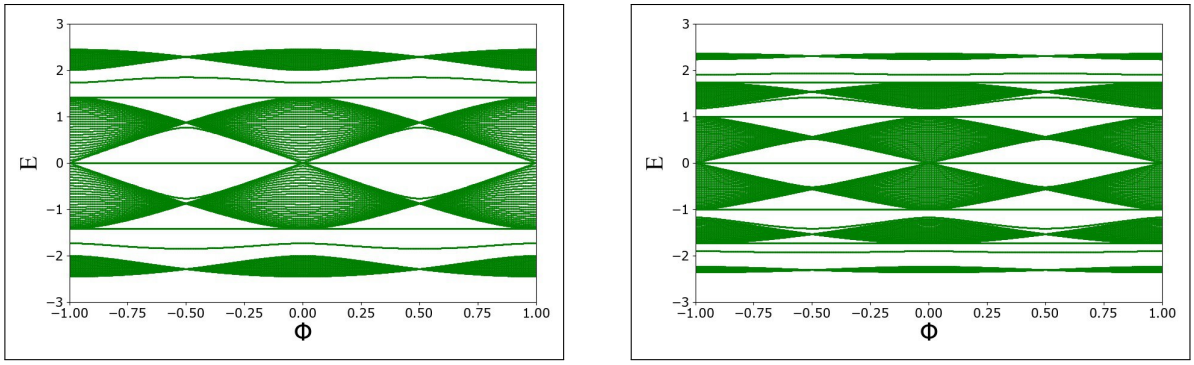

(a) (b)

Figure:7(a) allowed eigenspectrum of axially coupled diamond chain with number of atomic sites along each arm: N=1 (total number of atomic sites for plotting is 421) and N=2 (total number of atomic sites for plotting is 441)

There is a tendency of clustering of the eigenvalues towards the edges of the spectrum as is evident from the $E - \Phi$ diagram. Multiple inter-twined band crossings are noticed and the spectrum exhibits kind of a zero band gap semiconductor like behavior, mimicking a Dirac point as seen in graphene, at $\Phi = \pm\Phi_0$. The central gap gets gradually filled up by more eigenstates, and the $E - \Phi$ contours get more flattened up as N increases. At half flux the spectrum the spectrum consists of discrete set of data points. This leads to the interesting effect of extreme localization of eigenstates. This is true for any value of N, but the number of discrete data points increases depending upon the choice of N.

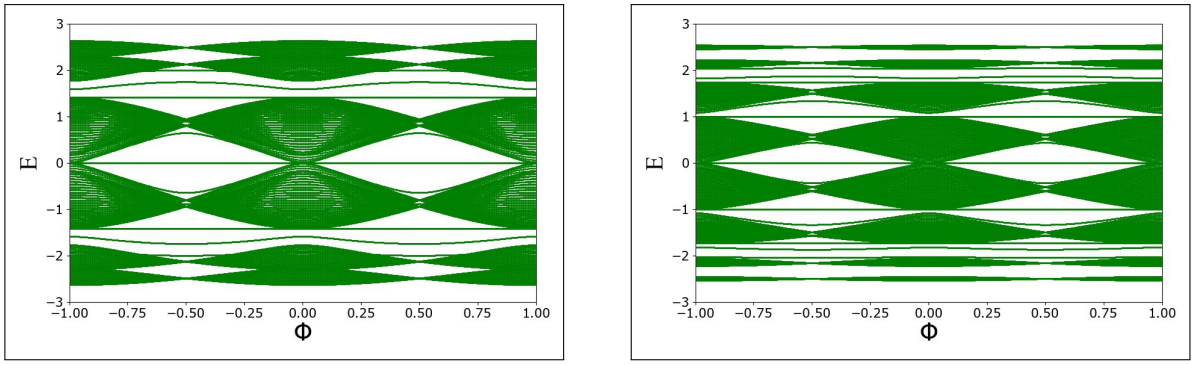

(a) (b)

Figure:7(b) allowed eigenspectrum of transverse coupled diamond chain with vertical hopping: t=1 and with number of atomic sites along each arm: N=1(total number of atomic sites for plotting is 421) and N=2(total number of atomic sites for plotting is 661)

E. Discussion of spectrum for the transversely coupled quantum rings

We have also plotted the allowed eigenvalues for the transverse coupled array of quantum rings as a function of the ratio of axial and transverse hoppings. The pattern is plotted for different flux combinations.

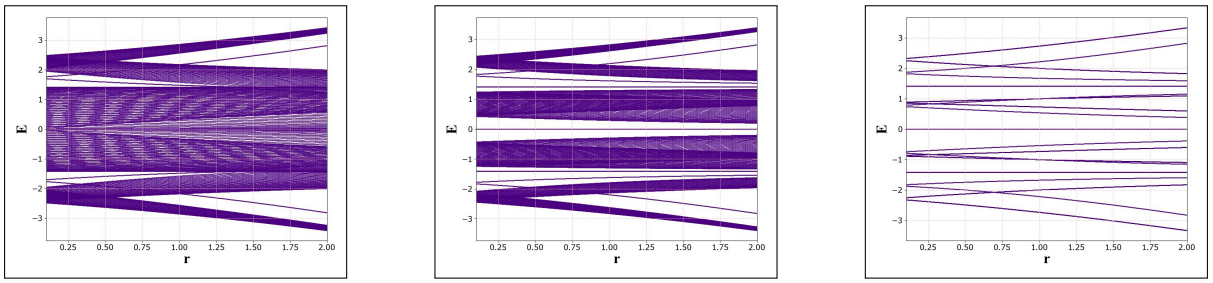

(a) (b) (c)

Figure: 8(a) variation of energy eigenvalues with respect to the ratio of inter-arm hopping for the transverse coupled diamond chain with uniform magnetic flux Φ (in units of $\Phi_0 = \frac{hc}{e}$), threaded by each plaquette, the value of magnetic flux is- (a) Φ= 0, (b) Φ= $\frac{1}{4}$, (c) Φ= $\frac{1}{2}$; with number of atomic sites along each arm of diamond: N=1, r denotes the ratio of axial and transverse couplings.

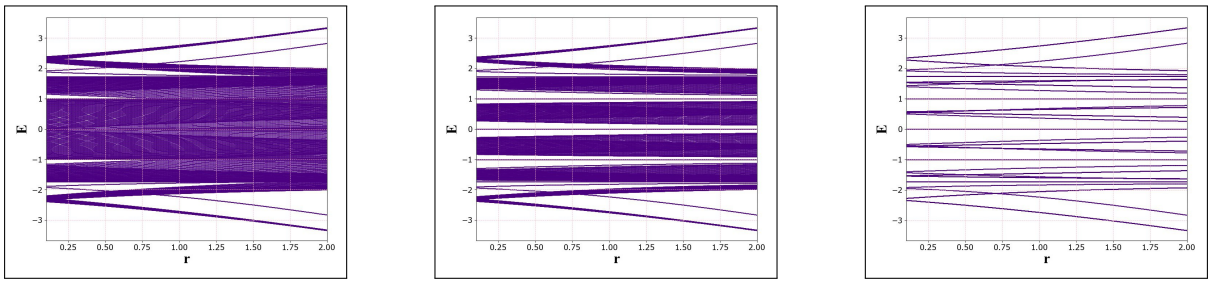

(a) (b) (c)

Figure: 8(b) variation of the same as mentioned in the upper panel, the value of the magnetic flux is- (d) Φ= 0, (e) Φ= $\frac{1}{4}$, (f) Φ= $\frac{1}{2}$; with number of atomic sites along each arm of diamond: N=2

Almost quasi-continuous pattern is seen in absence of flux. This in turn in presence of flux incorporates a number of gaps in between which ultimately leads to the case of AB caging for half flux quantum. The edge modes are also seen in presence of magnetic flux.

Conclusive remarks

In this work, we investigated the spectral properties of axially and transversely coupled quantum rings, emphasizing the effects of magnetic flux on the density of states (DOS) and inverse participation ratio (IPR). Through our analysis, several key insights emerged:

1. Spectral Fragmentation and Magnetic Flux:

The introduction of a magnetic flux through the quantum rings significantly alters the energy spectrum, inducing gaps and modifying the localization properties of the states. The presence of a flux breaks the time-reversal symmetry, leading to the Aharonov-Bohm effect, where the wave function of an electron gains a phase when traversing a closed loop. This phase shift is reflected in the fragmentation of the density of states, especially at critical flux values such as $\frac{\Phi_0}{2}$, where extreme localization of states is observed.

2. Density of States and Localization:

The density of states analysis revealed that in the absence of a magnetic flux, the spectrum consists of a central continuous band flanked by subbands, with a central spike indicating compact localization. As the magnetic flux increases, the continuous band bifurcates, and the central spike separates from the continuum, highlighting the magnetic flux's role in controlling the localization characteristics of the states. This behavior is particularly relevant for designing quantum devices where selective localization and delocalization of states are desired.

3. Inverse Participation Ratio as a Localization Measure:

The inverse participation ratio calculations supported the density of states findings by providing a quantitative measure of localization. The inverse participation ratio was highest for localized states and approached zero for extended states. The magnetic flux was shown to enhance localization, particularly at $\frac{\Phi_0}{2}$, where the system exhibited Aharonov-Bohm caging, a phenomenon where the electronic states are confined to a small region, leading to extreme localization.

4. Practical Implications:

The tunability of the spectral properties through magnetic flux makes these quantum ring arrays promising candidates for advanced nanotechnological applications. The ability to control the electronic properties through external parameters such as magnetic flux could lead to the development of novel quantum devices, including spin filters [33] and quantum switches [34] , where precise control over electron localization is crucial. Moreover, the potential to halt light propagation using Lieb [35] , diamond [36] , and other photonic lattices through Aharonov-Bohm caging further underscores the promise of these structures

in the design of photonic devices where control over light-matter interactions is essential.

In conclusion, this study highlights the intricate relationship between magnetic flux and the spectral properties of quantum ring arrays. The insights gained from this analysis provide a foundation for further exploration of quantum systems with potential applications in nanoscale electronics and quantum information processing. The observed phenomena, such as spectral fragmentation and Aharonov-Bohm caging, underscore the importance of magnetic flux in modulating the quantum behavior of electron systems, offering new avenues for experimental and theoretical research in condensed matter physics.

Bibliography

[1] A. Aharony et al. “Title of the Article”. In: *Physical Review Letters* (2001).

[2] M. Scheid et al. “Title of the Article”. In: *Physical Review B* 76.19 (2007), p. 195303.

[3] J. Vidal et al. “Title of the Article”. In: *Physical Review B* 64 (2001), p. 155306.

[4] F. Bloch. “Title of the Article”. In: *Z. Phys.* 52 (1928), p. 555.

[5] P. W. Anderson. “Title of the Article”. In: *Phys. Rev.* 109 (1958), p. 1942.

[6] D. C. Licciardello and D. J. Thouless. “Title of the Article”. In: *J. Phys. C* 8 (1975). J. Phys. C 11, 925 (1978), p. 4157.

[7] P. A. Lee and T. V. Ramakrishnan. “Title of the Article”. In: *Rev. Mod. Phys.* 57 (1985), p. 287.

[8] P. Sheng, ed. *Scattering and Localization of Classical Waves in Random Media*. World Scientific Series on Directions in Condensed Matter Physics: Volume 8. World Scientific, 1990.

[9] S. John. “Title of the Article”. In: *Phys. Rev. Lett.* 53 (1984). Phys. Rev. Lett. 58, 2486 (1987), p. 2169.

[10] A. Klein and A. Koines. “Title of the Article”. In: *Mathematical Physics, Analysis and Geometry* 7 (2004). and references therein, p. 151.

[11] D. M. Jović et al. “Title of the Article”. In: *Phys. Rev. A* 83 (2011), p. 033813.

[12] A. A. Asatryan et al. “Title of the Article”. In: *Phys. Rev. B* 81 (2010). Phys. Rev. B 85, 045122 (2012), p. 075124.

[13] P. Sheng and Z. Q. Zhang. “Title of the Article”. In: *Phys. Rev. Lett.* 57 (1986), p. 1879.

[14] C. A. Condat and T. R. Kirkpatrick. “Title of the Article”. In: *Phys. Rev. B* 36 (1987). Phys. Rev. Lett. 58, 226 (1987), p. 6782.

[15] S. He and J. D. Maynard. “Title of the Article”. In: *Phys. Rev. Lett.* 57 (1986), p. 3171.

[16] Z. Shi and A. Z. Genack. “Title of the Article”. In: *Phys. Rev. Lett.* 108 (2012), p. 043901.

[17] R. Dalichaouch et al. “Title of the Article”. In: *Nature* 354 (1991), p. 53.

[18] D. S. Wiersma et al. “Title of the Article”. In: *Nature* 390 (1997), p. 671.

[19] H. Hu et al. “Title of the Article”. In: *Nat. Phys.* 4 (2008), p. 945.

[20] J. Billy et al. “Title of the Article”. In: *Nature* 453 (2008), p. 891.

[21] G. Roati et al. “Title of the Article”. In: *Nature* 453 (2008), p. 895.

[22] Y. Aharonov and D. Bohm. “Title of the Article”. In: *Phys. Rev.* 115 (1959), p. 485.

[23] C. Benjamin and A. M. Jayannavar. “Title of the Article”. In: *Phys. Rev. B* 68 (2003), p. 085325.

[24] M. Yamamoto et al. “Title of the Article”. In: *Nature Nanotech.* 7 (2012), p. 247.

[25] B. Kubala and J. König. “Title of the Article”. In: *Phys. Rev. B* 65 (2002), p. 245301.

[26] F. E. Camino, W. Zhou, and V. J. Goldman. “Title of the Article”. In: *Phys. Rev. B* 72 (2005), p. 155313.

[27] V. Moldoveanu et al. “Title of the Article”. In: *Phys. Rev. B* 71 (2005), p. 125338.

[28] D. Mondal et al. “Title of the Article”. In: *Applied Materials Today* 40 (2024), p. 102360. DOI: 10.1016/j.apmt.2024.102360.

[29] A. Mukherjee et al. “Title of the Article”. In: *Journal of Physics: Condensed Matter* 33.3 (2024). DOI: 10.1088/1361-648X/abbc9a.

[30] A. Alexandrov and H. Capellmann. “Title of the Article”. In: *Z. Phys. B* 83 (1991), p. 237.

[31] M. Di Liberto et al. “Aharonov-Bohm cages: Topology, degeneracy, and flat bands”. In: *Physical Review A* 100.4 (2019), p. 043829. DOI: 10.1103/PhysRevA.100.043829.

[32] H.-F. Cheung et al. “Title of the Article”. In: *Phys. Rev. B* 37 (1988), p. 6050.

[33] T. Koga et al. “Title of the Article”. In: *Physical Review Letters* 88.12 (2002), p. 126601.

[34] M. Scheid et al. “Title of the Article”. In: *Physical Review B* 76.19 (2007), p. 195303.

[35] S. Mukherjee et al. *Observation of a localized flat-band state in a photonic Lieb lattice*. physics.optics. 2018. eprint: `arXiv:1412.6342v3`.

[36] S. Mukherjee et al. *Experimental observation of AB cages in photonic lattice*. physics.optics. 2018. eprint: `arXiv:1805.03564v2`.

Appendix

Appendix- A

The decimation scheme

From the difference equation (**see Appendix-E**):

$$(E-\epsilon)\psi_A = t_F\psi_1 + t_B\psi_{-1} + t_F\psi_{-n} \tag{21}$$
$$(E-\epsilon)\psi_1 = t_B\psi_A + t_F\psi_2 \tag{22}$$
$$(E-\epsilon)\psi_2 = t_B\psi_1 + t_F\psi_3 \tag{23}$$

Now these difference equations for the coupled system can be easily written in the matrix from using the potential parameters-

$$\begin{pmatrix}\Psi_2\\ \Psi_1\end{pmatrix} = \begin{pmatrix}\frac{(E-\epsilon)}{t_f} & -\frac{t_b}{t_f}\\ 1 & 0\end{pmatrix}\begin{pmatrix}\Psi_1\\ \Psi_A\end{pmatrix} \tag{24}$$

where,

$$M = \begin{pmatrix}\frac{(E-\epsilon)}{t_f} & -\frac{t_b}{t_f}\\ 1 & 0\end{pmatrix} \tag{25}$$

Here, M is the transfer matrix. again,

$$\begin{pmatrix}\psi_3\\ \psi_2\end{pmatrix} = M\begin{pmatrix}\psi_2\\ \psi_1\end{pmatrix} = M^2\begin{pmatrix}\psi_1\\ \psi_A\end{pmatrix} \tag{26}$$

similarly,

$$\begin{pmatrix}\psi_B\\ \psi_3\end{pmatrix} = M\begin{pmatrix}\psi_3\\ \psi_2\end{pmatrix} = M^3\begin{pmatrix}\psi_1\\ \psi_A\end{pmatrix} \tag{27}$$

in this way we can ultimately write,

$$\begin{pmatrix}\psi_B\\ \psi_N\end{pmatrix} = M^N\begin{pmatrix}\psi_1\\ \psi_A\end{pmatrix} \tag{28}$$

$$\begin{pmatrix}\psi_B\\ \psi_N\end{pmatrix} = \begin{pmatrix}M_{11}^N & M_{12}^N\\ M_{21}^N & M_{22}^N\end{pmatrix}\begin{pmatrix}\psi_1\\ \psi_A\end{pmatrix} \tag{29}$$

it can be shown that,

$$M^N = e^{-i(N-1)\theta}\left[U_{N-1}(x)M - e^{-i\theta}U_{N-2}(x)\mathbb{I}\right] \tag{30}$$

Now,

$$M = \begin{pmatrix}\frac{(E-\epsilon)}{t}e^{-}i\theta & -e^{-}2i\theta\\ 1 & 0\end{pmatrix} \tag{31}$$

where,

$$x = \frac{E-\epsilon}{2t} \tag{32}$$

from equation,

$$\psi_B = M_{11}^N\psi_1 + M_{12}^N\psi_A \tag{33}$$

now,

$$M^N = e^{-i(N-1)\theta}U_{\text{N-1}}\begin{pmatrix}2xe^{-i\theta} & -e^{-2i\theta}\\ 1 & 0\end{pmatrix} - e^{-iN\theta}U_{\text{N-2}}\begin{pmatrix}1 & 0\\ 0 & 1\end{pmatrix} \tag{34}$$

$$M^N = e^{-iN\theta}\begin{pmatrix} 2xe^{-i\theta}U_{\text{N-1}} & -e^{-2i\theta}U_{\text{N-1}} \\ e^{i\theta}U_{\text{N-1}} & 0 \end{pmatrix} - e^{-iN\theta}\begin{pmatrix} U_{\text{N-2}} & 0 \\ 0 & U_{\text{N-2}} \end{pmatrix} \tag{35}$$

$$M^N = e^{-iN\theta}\begin{pmatrix} 2xU_{\text{N-1}} - U_{\text{N-2}} & -e^{-i\theta}U_{\text{N-1}} \\ e^{i\theta}U_{\text{N-1}} & -U_{\text{N-2}} \end{pmatrix} \tag{36}$$

$$M^N = e^{-iN\theta}\begin{pmatrix} U_{\text{N}} & -e^{-i\theta}U_{\text{N-1}} \\ e^{i\theta}U_{\text{N-1}} & -U_{\text{N-2}} \end{pmatrix} \tag{37}$$

hence, for upper arm of the plaquette,

$$\psi_1^{\text{up}} = \frac{1}{M_{11}^N}\psi_B - \frac{M_{12}^N}{M_{11}^N}\psi_A \tag{38}$$

$$\psi_1^{\text{up}} = \frac{e^{iN\theta}}{U_N}\psi_B + e^{-i\theta}\frac{U_{\text{N-1}}}{U_N}\psi_A \tag{39}$$

similarly,for down arm-

$$\psi_1^{\text{down}} = \frac{e^{-iN\theta}}{U_N}\psi_D + e^{+i\theta}\frac{U_{\text{N-1}}}{U_N}\psi_A \tag{40}$$

now, the difference equation takes the from:

$$(E-\epsilon)\psi_A = te^{i\theta}\psi_1^{\text{up}} + te^{-i\theta}\psi_1^{\text{down}} \tag{41}$$

$$(E-\epsilon)\psi_A = te^{i\theta}[\frac{e^{iN\theta}}{U_N}\psi_B + e^{-i\theta}\frac{U_{\text{N-1}}}{U_N}\psi_A] + te^{-i\theta}[\frac{e^{-iN\theta}}{U_N}\psi_D + e^{+i\theta}\frac{U_{\text{N-1}}}{U_N}\psi_A] \tag{42}$$

$$[E-(\epsilon + \frac{2tU_{\text{N-1}}}{U_N})]\psi_A = \frac{te^{\text{i(N+1}\theta}}{U_N}\psi_B + \frac{te^{\text{-i (N+1}\Theta}}{U_N}\psi_D \tag{43}$$

$$[E-\tilde{\epsilon}]\psi_A = \tilde{t_F}\psi_B + \tilde{t_B}\psi_D \tag{44}$$

Appendix- B

Chebysheb polynomials

The **Chebyshev polynomials of the second kind** are defined by the recurrence relation:

$$U_0(x) = 1 \tag{45}$$
$$U_1(x) = 2x \tag{46}$$
$$U_{n+1}(x) = 2xU_n(x) - U_{n-1}(x) \tag{47}$$

Notice that the two sets of recurrence relations are identical, except for $T_1(x) = x$ vs. $U_1(x) = 2x$. The ordinary generating function for U_n is:

$$\sum_{n=0}^{\infty} U_n(x)t^n = \frac{1}{1 - 2tx + t^2}, \tag{48}$$

and the exponential generating function is:

$$\sum_{n=0}^{\infty} \frac{U_n(x)t^n}{n!} = e^{tx}\left(\cosh\left(t\sqrt{x^2-1}\right) + \frac{x}{\sqrt{x^2-1}}\sinh\left(t\sqrt{x^2-1}\right)\right). \tag{49}$$

The **Chebyshev polynomials of the second kind** are defined by the recurrence relation:

$$U_0(x) = 1 \tag{50}$$
$$U_1(x) = 2x \tag{51}$$
$$U_{n+1}(x) = 2xU_n(x) - U_{n-1}(x) \tag{52}$$

Notice that the two sets of recurrence relations are identical, except for $T_1(x) = x$ vs. $U_1(x) = 2x$. The ordinary generating function for U_n is:

$$\sum_{n=0}^{\infty} U_n(x)t^n = \frac{1}{1 - 2tx + t^2}, \tag{53}$$

and the exponential generating function is:

$$\sum_{n=0}^{\infty} \frac{U_n(x)t^n}{n!} = e^{tx}\left(\cosh\left(t\sqrt{x^2-1}\right) + \frac{x}{\sqrt{x^2-1}}\sinh\left(t\sqrt{x^2-1}\right)\right). \tag{54}$$

The first few ChebyShev polynomial of second kind are:

$$U_0(x) = 1$$
$$U_1(x) = 2x$$
$$U_2(x) = 4x^2 - 1$$
$$U_3(x) = 8x^3 - 4x$$
$$U_4(x) = 16x^4 - 12x^2 + 1$$
$$U_5(x) = 32x^5 - 32x^3 + 6x$$
$$U_6(x) = 64x^6 - 80x^4 + 24x^2 - 1$$
$$U_7(x) = 128x^7 - 192x^5 + 80x^3 - 8x$$
$$U_8(x) = 256x^8 - 448x^6 + 240x^4 - 40x^2 + 1$$
$$U_9(x) = 512x^9 - 1024x^7 + 672x^5 - 160x^3 + 10x$$
$$U_{10}(x) = 1024x^{10} - 2304x^8 + 1792x^6 - 560x^4 + 60x^2 - 1 \tag{55}$$

Appendix- C

Peierls' phase factor

In this segment, we will show the Peierls' phase factor associated with the hopping integral parameter when an electron traverses a close loop experienced a uniform magnetic flux Φ,the overlap integral t between two atomic sites n and $(n+1)$ in a lattice is given by:

$$t \equiv t_{n,n+1} = \langle \psi_n | H | \psi_{n+1} \rangle = \langle \psi_m | H | \psi_{m+1} \rangle \tag{56}$$

where, ψ_n is the wave function amplitude at the respective quantum dot position. If the electron is travelling along a closed path in a region where non-zero magnetic vector potential $\mathbf{A}$ exists, then the acquired phase shift by the wave function is given by:

$$\psi_n = \psi_n^0 \exp\left[\frac{iq}{\hbar}\int_{na}^{na+\mathbf{R}} \mathbf{A}\cdot d\mathbf{l}\right] \tag{57}$$

$$\psi_{n+1} = \psi_{n+1}^0 \exp\left[\frac{iq}{\hbar}\int_{(n+1)a}^{na+\mathbf{R}} \mathbf{A}\cdot d\mathbf{l}\right] \tag{58}$$

where,$(na+\mathbf{R})$ is some final point within the lattice, a is the lattice periodicity, q is the charge of the electron, and $\hbar$ is the reduced Planck's constant. Therefore, we obtain:

$$t \equiv t_{n,n+1} = \langle \psi_n^0 \exp\left[\frac{iq}{\hbar}\int_{na}^{na+\mathbf{R}} \mathbf{A}\cdot d\mathbf{l}\right] |t| \psi_{n+1}^0 \exp\left[\frac{iq}{\hbar}\int_{(n+1)a}^{na+\mathbf{R}} \mathbf{A}\cdot d\mathbf{l}\right] \rangle \tag{59}$$

This in turn reduces on further simplification to the following form:

$$t_{n,n+1} = \langle \psi_n^0 \exp\left[\frac{iq}{\hbar}\int_{na}^{na+\mathbf{R}} \mathbf{A}\cdot d\mathbf{l}\right] |t| \psi_{n+1}^0 \exp\left[-\frac{iq}{\hbar}\int_{(n+1)a}^{na+\mathbf{R}} \mathbf{A}\cdot d\mathbf{l}\right] \rangle \tag{60}$$

$$t_{n,n+1} = \int \psi_n^0 t \psi_{n+1}^0 \exp\left[\frac{iq}{\hbar}\int_{na}^{(n+1)a} \mathbf{A}\cdot d\mathbf{l}\right] \tag{61}$$

$$t_{n,n+1} = t_{n,n+1}^0 \exp(-i\theta) \tag{62}$$

$$t_{n,n+1} = t^0 \exp(-i\theta) \tag{63}$$

where,

$$\theta = \frac{q}{\hbar}\int_{na}^{(n+1)a} \mathbf{A}\cdot d\mathbf{l} = \frac{2\pi\Phi}{\frac{h}{q}} = \frac{2\pi\Phi}{\Phi_0} \tag{64}$$

is the required Peierls' phase factor. $\Phi_0 = \frac{h}{q}$ is called the fundamental flux quantum. It is needless to say that one can easily compute the integral in the above equation (82) by virtue of Stokes' theorem and the fact that $\mathbf{B} = \nabla \times \mathbf{A}$.

Appendix- D

Derivation of local density of states

By definition, we have:

$$(E-H)G = I \Rightarrow G = \frac{I}{E-H} \Rightarrow G = \frac{\sum_k |k\rangle\langle k|}{E-H} \tag{65}$$

$$\Rightarrow G = \sum_K (E-H)^{-1}|k\rangle\langle k| \tag{66}$$

Expanding the right hand side of the last equation, we obtain:

$$G = \sum_K (E + H + H^2 + \ldots)|k\rangle\langle k| \tag{67}$$

$$\Rightarrow G = \sum_K \left[E + \epsilon(k) + \epsilon(k)^2 + \ldots\right]|k\rangle\langle k| \tag{68}$$

$$G = \sum_k \frac{|k\rangle\langle k|}{E - \epsilon(k)} \tag{69}$$

Therefore,we can easily write,

$$\langle m|G|n\rangle \equiv G_{mn} = \sum_k \frac{\langle m|k\rangle\langle k|n\rangle}{E - \epsilon(k)} \tag{70}$$

Bloch basis $|k\rangle$ is related to the Wannier basis $|n\rangle$ by a Fourier-transform relation as follows:

$$|k\rangle = \frac{1}{\sqrt{N}} \sum_n e^{ikna}|n\rangle \tag{71}$$

We can compute,

$$\langle m|k\rangle = \frac{1}{\sqrt{N}} \sum_n e^{ikna}\langle m|n\rangle \tag{72}$$

$$\langle m|k\rangle = \frac{1}{\sqrt{N}} \sum_n e^{ikna}\delta_{mn} \tag{73}$$

$$\langle m|k\rangle = \frac{1}{\sqrt{N}} e^{ikma} \tag{74}$$

In an exactly similar fashion, we can easily write,

$$\langle k|n\rangle = \frac{1}{\sqrt{N}} e^{-ikna} \tag{75}$$

We obtain the off-diagonal term of Green's function (non-local Green's function) as,

$$G_{mn} = \frac{1}{N} \sum_k \frac{e^{ik(m-n)a}}{E - \epsilon(k)} \tag{76}$$

Local Green's function can be written by putting $m = 0 = n$ in the above expression as,

$$G_{00}(E) = \frac{1}{N}\sum_{k}\frac{1}{E-\epsilon(k)} \tag{77}$$

$$\Rightarrow G_{00}(E+i\eta) = \frac{1}{N}\sum_{k}\frac{1}{E+i\eta-\epsilon(k)} \tag{78}$$

Where $\eta \to 0^{+}$, Now,

$$\frac{1}{(E+i\eta-\epsilon(k))} = P\left(\frac{1}{(E-\epsilon(k))}\right) - i\pi\delta[E-\epsilon(k)] \tag{79}$$

$$\Rightarrow \frac{1}{N}\sum_{k}\delta[E-\epsilon(k)] = -\frac{1}{\pi}\mathrm{Im}G_{00} \tag{80}$$

So, finally we can have the well-known expression for the local density of states as follows:

$$\rho_{00}(E) = \lim_{\eta\to 0^{+}}\left[-\frac{1}{\pi}\mathrm{Im}(G_{00}(E+i\eta))\right] \tag{81}$$

Appendix- E

The difference equation

In this section, we will show the detailed derivation of the difference equation which is also an alternative discretized version of time independent Schrodinger's equation. This basic equation we have used several times to express the dynamics of electron across the lattice network.

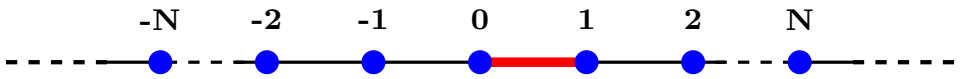

Figure: 9 Schematic diagram of a one dimensional perfectly periodic lattice

For this purpose, we need to consider a one dimensional (1D) periodic chain of atomic sites with the periodicity 'a' i.e., distance between two consecutive atomic sites as shown in Figure 9. Now the well-known Schrodinger's equation is given by:

$$-\frac{\hbar^2}{2m}\frac{d^2\psi(x)}{dx^2} + V(x)\psi(x) = E\psi(x) \tag{82}$$

It is needless to say that the first part gives the kinetic information, $V(x)$ carries the potential structure and E gives the total energy of the particle. Let us now mark the different quantum dot notation as shown in **Figure(9)**. If ψ_n be the wave function amplitude at the n^{th} atomic site and V_n be the potential at the corresponding atomic site position, then mathematically we can write:

$$\left[\frac{d\psi}{dx}\right]_{x=(n+\frac{1}{2})a} = \frac{\psi_{n+1} - \psi_n}{a} \tag{83}$$

$$\left[\frac{d\psi}{dx}\right]_{x=(n-\frac{1}{2})a} = \frac{\psi_n - \psi_{n-1}}{a} \tag{84}$$

$$\left[\frac{d^2\psi}{dx^2}\right]_{x=na} = \frac{\left[\frac{d\psi}{dx}\right]_{x=(n+\frac{1}{2})a} - \left[\frac{d\psi}{dx}\right]_{x=(n-\frac{1}{2})a}}{a} \tag{85}$$

$$\left[\frac{d^2\psi}{dx^2}\right]_{x=na} = \frac{1}{a^2}(\psi_{n+1} - \psi_n - \psi_n + \psi_{n-1}) \tag{86}$$

$$\left[\frac{d^2\psi}{dx^2}\right]_{x=na} = \frac{1}{a^2}(\psi_{n+1} - 2\psi_n + \psi_{n-1}) \tag{87}$$

hence, we can obtain:

$$-\frac{\hbar^2}{2ma^2}[\psi_{n+1} - 2\psi_n + \psi_{n-1}] + v_n(x)\psi_n(x) = E\psi_n(x) \tag{88}$$

$$-\frac{\hbar^2}{2ma^2}[\psi_{n+1} + \psi_{n-1}] = \left[E - \left(v_n + \frac{\hbar^2}{2ma^2}\right)\right]\psi_n(x) \tag{89}$$

$$(E - \epsilon_n)\psi_n = t_{n,n+1}\psi_{n+1} + t_{n,n-1}\psi_{n-1} \tag{90}$$

$$t_{n,n+1} = t_{n,n-1} = -\frac{\hbar^2}{2ma^2} \tag{91}$$

$$\epsilon_n = \left(v_n + \frac{\hbar^2}{2ma^2}\right) \tag{92}$$

$$t = t_{n,n+1} = t_{n,n-1} = -\frac{\hbar^2}{2ma^2} \tag{93}$$

where ϵ_n represents the onsite potential and t is the overlap parameter of electron across the lattice network.

Sample codes

```
# Python code for axially coupled array of diamond ring with number of atomic
sites in each arm is: N=1

# Code for "density of states" plotting

import numpy as np
import matplotlib.pyplot as plt

import numpy as np
import matplotlib.pyplot as plt

# parameters for calculation
eim = 0.001
eps = 0.00001
Nm =30
Nsys = 7 * Nm + 1
list1 = []
est = -4.0
emax = 4.0
eint = 0.01
phi=0
theta=(np.pi*phi)/4
tf=np.exp(+1j*theta)
tb=np.exp(-1j*theta)

# Calculate density of states
for eng in np.arange(est, emax, eint):
    e = eng + 1j * eim
    emat = np.eye(Nsys) * e
    mat = np.eye((Nsys), dtype=complex)*eps

    for i in range(1, Nm):
        mat[7*i - 6 , 7*i - 5] = (tb)
        mat[7*i - 5, 7*i - 6] = (tf)

        mat[7*i - 5, 7*i - 3] = (tb)
        mat[7*i - 3, 7*i - 5] = (tf)

        mat[7*i - 3, 7*i - 1] = (tb)
        mat[7*i - 1, 7*i - 3] = (tf)

        mat[7*i - 1, 7*i + 1] = (tb)
        mat[7*i + 1 ,7*i - 1] = (tf)

        mat[7*i - 6 , 7*i - 4] = (tf)
        mat[7*i  - 4,  7*i - 6] = (tb)

        mat[7*i - 4, 7*i - 2] = (tf)
        mat[7*i - 2, 7*i - 4] = (tb)

        mat[7*i - 2, 7*i ] = (tf)
        mat[7*i , 7*i - 2] = (tb)

        mat[7*i , 7*i + 1] = (tf)
        mat[7*i + 1, 7*i ] = (tb)



    effmat = emat - mat
```

```
    greenmat = np.linalg.inv(effmat)
    trmat = np.trace(greenmat)
    multi = Nsys
    dos = (-1 / (multi*np.pi)) * np.imag(trmat)

    list1.append([eng, dos])

# Plotting
eng_values = [pair[0] for pair in list1]
dos_values = [pair[1] for pair in list1]

plt.figure(figsize=(8, 6))
plt.plot(eng_values, dos_values, color='red', linewidth=1.5)
plt.xlabel('E', fontsize=29, fontname='Times New Roman', fontweight='bold')
plt.ylabel('ρ', fontsize=29, fontname='Times New Roman', fontweight='bold')
plt.xticks(fontsize=20)
plt.yticks(fontsize=15)
plt.grid(True, linestyle='--', color='pink')
plt.xlim(min(eng_values), max(eng_values))
plt.ylim(0,2)
plt.show()


# Code for "inverse participation ratio" plotting

import numpy as np
import matplotlib.pyplot as plt

# parameters for calculation
eim = 0.001
eps = 0.00001
Nm = 100
Nsys = 7 * Nm + 1
phi = 0
theta = (np.pi * phi) / 4
tf = 1 * np.exp(+1j * theta)
tb = 1 * np.exp(-1j * theta)

# Construct the Hamiltonian matrix
mat = np.eye(Nsys, dtype=complex ) * eps

for i in range(1, Nm):
        mat[7*i - 6 , 7*i - 5] = (tb)
        mat[7*i - 5, 7*i - 6] = (tf)

        mat[7*i - 5, 7*i - 3] = (tb)
        mat[7*i - 3, 7*i - 5] = (tf)

        mat[7*i - 3, 7*i - 1] = (tb)
        mat[7*i - 1, 7*i - 3] = (tf)

        mat[7*i - 1, 7*i + 1] = (tb)
        mat[7*i + 1 ,7*i - 1] = (tf)

        mat[7*i - 6 , 7*i - 4] = (tf)
        mat[7*i  - 4,  7*i - 6] = (tb)

        mat[7*i - 4, 7*i - 2] = (tf)
        mat[7*i - 2, 7*i - 4] = (tb)
```

```
        mat[7*i - 2, 7*i ] = (tf)
        mat[7*i , 7*i - 2] = (tb)

        mat[7*i , 7*i + 1] = (tf)
        mat[7*i + 1, 7*i ] = (tb)



# Diagonalize the Hamiltonian matrix to find eigenvalues and eigenvectors
eigenvalues, eigenvectors = np.linalg.eigh(mat)


energy_I_list = []

# Calculate I for each wave function (eigenvector)
for idx in range(len(eigenvalues)):
    wave_function = eigenvectors[:, idx]
    #wave_function_squared = (wave_function)**2
    sum_psi_squared = np.sum(np.abs(wave_function) ** 2)
    sum_psi_fourth = np.sum(np.abs(wave_function) ** 4)

    I = sum_psi_fourth / (sum_psi_squared ** 2)
    energy_I_list.append([eigenvalues[idx], I])


energy_values = [pair[0] for pair in energy_I_list]
I_values = [pair[1] for pair in energy_I_list]

# Plotting
plt.figure(figsize=(8, 6))
plt.scatter(energy_values, I_values, color='blue', s=10)
plt.xlabel('E', fontsize=29, fontname='Times New Roman', fontweight='bold')
plt.ylabel('I', fontsize=29, fontname='Times New Roman', fontweight='bold')
plt.xticks(fontsize=20)
plt.yticks(fontsize=15)
plt.grid(True, linestyle='--', color='pink')
plt.ylim(0,1.1)
plt.xlim(-4,4)
plt.show()


# Code for "dispersion relation" plotting

import numpy as np
import matplotlib.pyplot as plt

# Parameters for calculation
t=1
a = 1
phi = 0
theta = (np.pi * phi) / 4
tb = t * np.exp(-1j * theta)
tf = t * np.exp(1j * theta)

# Function to create the Hamiltonian matrix for a given k
def create_hamiltonian(k):
    mat = np.zeros((7, 7), dtype=complex)
    mat[0, 1] = tb
```

```
    mat[1, 0] = tf
    mat[1, 3] = tb
    mat[3, 1] = tf
    mat[3, 5] = tb
    mat[5, 3] = tf
    mat[0, 5] = tf * np.exp(-1j * k * a)
    mat[5, 0] = tb * np.exp(+1j * k * a)
    mat[0, 2] = tf
    mat[2, 0] = tb
    mat[2, 4] = tf
    mat[4, 2] = tb
    mat[4, 6] = tf
    mat[6, 4] = tb
    mat[6, 0] = tf * np.exp(+1j * k * a)
    mat[0, 6] = tb * np.exp(-1j * k * a)
    return mat

# Generate 500 values of k from -pi to pi
k_values = np.linspace(0, 2* np.pi , 500)

# Calculate eigenvalues for each value of k
eigenvalues = []
for k in k_values:
    H = create_hamiltonian(k)
    eigvals = np.linalg.eigvals(H)
    eigvals = np.sort(eigvals)
    eigenvalues.append(eigvals)

# Convert eigenvalues list to a numpy array for easier plotting
eigenvalues = np.array(eigenvalues)

# Plotting
plt.figure(figsize=(10, 6))
for i in range(eigenvalues.shape[1]):
    plt.plot(k_values, eigenvalues[:, i].real, color='black')

plt.xlabel('k',fontname='Times new roman',fontsize=27, fontweight='normal')
plt.ylabel('E',fontname='Times new roman',fontsize=27, fontweight='normal')
plt.xlim(k_values[0], k_values[-1])
plt.xticks(fontsize=24)
plt.yticks(fontsize=24)
plt.show()
```